VALIDATION OF HIGH-FIDELITY CFD/CAA FRAMEWORK FOR LAUNCH VEHICLE ACOUSTIC ENVIRONMENT SIMULATION AGAINST SCALE MODEL TEST DATA

Peter A. Liever [1], Jeffrey S. West [2], Robert E. Harris [3]

[1] CFD Research Corporation, Jacobs ESSSA Group, NASA Marshall Space Flight Center
[2] NASA Marshall Space Flight Center
[3] CFD Research Corporation
Huntsville, AL

ABSTRACT

A hybrid Computational Fluid Dynamics and Computational Aero-Acoustics (CFD/CAA) modeling framework has been developed for launch vehicle liftoff acoustic environment predictions. The framework couples the existing highly-scalable NASA production CFD code, Loci/CHEM, with a high-order accurate Discontinuous Galerkin solver developed in the same production framework, Loci/THRUST, to accurately resolve and propagate acoustic physics across the entire launch environment. Time-accurate, Hybrid RANS/LES CFD modeling is applied for predicting the acoustic generation physics at the plume source, and a high-order accurate unstructured mesh Discontinuous Galerkin (DG) method is employed to propagate acoustic waves away from the source across large distances using high-order accurate schemes. The DG solver is capable of solving 2nd, 3rd, and 4th order Euler solutions for non-linear, conservative acoustic field propagation. Initial application testing and validation has been carried out against high resolution acoustic data from the Ares Scale Model Acoustic Test (ASMAT) series to evaluate the capabilities and production readiness of the CFD/CAA system to resolve the observed spectrum of acoustic frequency content. This paper presents results from this validation and outlines efforts to mature and improve the computational simulation framework.

INTRODUCTION

Space launch vehicles experience high acoustic loads during ignition and liftoff. Launch vehicle acoustic loads can be subdivided into two distinct mechanisms: 1) low frequency, large amplitude, finite waves such as ignition over-pressure waves during startup of liquid engines and solid motors; and 2) broad range noise generated by the supersonic plume shear layers and plume impingement regions on the launch platform and the flame trench. Both create high sound-pressure level loads along the vehicle including the payload and crew sections.

The rocket plume noise originates from supersonic plume shear layers as broad range and directional Mach wave acoustic radiation. Plume impingement on the launch platform as the vehicle ascends and the plumes spill and impinge on the deck generates new sources of noise, as does the plume impingement in the flame trench, noise propagation around the launch platform, and noise from the plumes exiting the flame trench. Peak plume noise occurs late in the liftoff phase, as the vehicle aft end rises to tower level, the plumes emerge from the launch pad flame holes and the plume noise waves are reflected by the launch pad towards the vehicle. Mitigation measures consist primarily of injection of sound suppression deluge water onto the deck that suppresses the noise reflection and also dampens plume impingement noise sources. These loads are strongly affected by the interaction of the rocket plume's acoustic waves with the launch pad structure.

Computational Fluid Dynamics (CFD) methods are now capable of running large-scale models using thousands of processors on NASA supercomputers. CFD analyses of complete

launch vehicles with multiple plumes interacting with full launch pad geometric models are now performed routinely at NASA's Marshall Space Flight Center (MSFC) in support of liftoff environments analysis. These analyses helped define liftoff environments for the Space Shuttle and for current launch vehicle designs such as the Space Launch System (SLS).

CFD modeling must be capable of modeling the plume noise source mechanisms and plume impingement and spillage noise source regions across the frequency band of interest, which extends from low frequencies to beyond 5000 Hz. Properly resolved CFD simulations require time-accurate hybrid RANS/LES modeling for multiple plumes with diverse plume gas composition embedded in a detailed launch pad model to capture the noise interaction with the pad structures. As deluge water injection is the main mitigation measure, CFD simulations must also be able to model the effects of the presence of water. Flow solver algorithms capable of performing simulations with flow physics of this complexity are typically second order accurate at best with considerable numerical dissipation for robustness. They are by nature tailored towards providing robust engineering analyses of complex propulsion flow field effects. Performing direct propagation of the acoustic waves originating from the resulting flow features requires considerably higher resolution and numerical accuracy.

TWO-FIELD CFD/CAA APPROACH FOR LIFTOFF ACOUSTICS ANALYSIS

Propagating the acoustic waves and their full frequency content accurately over large simulation domains requires a Computational Aero-Acoustics (CAA) field solution that is non-dissipative with high order accurate wave tracking, capable of resolving and preserving frequency content from low frequency ignition pulses to high frequency acoustics in the kilo-Hertz range. It is currently not possible to simultaneously satisfy the robust plume flow solver requirements and the high accuracy requirements of the CAA solver within a single flow solver algorithm. The apparent solution is a hybrid approach that performs distinct CFD and CAA solution processes in which the acoustic field from the plume flow solver source regions is transmitted to a specialized acoustic field propagation solver. The proper selection of the CAA method for NASA liftoff acoustics analysis is driven by the need to capture and resolve the interference effects in the acoustic field propagation from the presence of launch structures such as the launch platform and the access tower.

Acoustic field prediction methods are ubiquitous in the CAA modeling community, but numerous different simplified equation sets are often used to model the acoustics. Many of these approaches are so-called acoustic analogies. These include the original analogy of Lighthill [1] [2], Kirchhoff's method [3], Ffowcs-Williams-Hawkings (FWH) method [4], boundary element methods (BEM) [5], linearized Euler equations (LEE) [6] [7] [8], and acoustic perturbation equations (APE) [8] [9]. Kirchhoff and FWH formulations have often been favored for many free jet noise predictions, which are characterized by acoustic propagation through an unobstructed field. However, both of these approaches are unable to accommodate physical obstructions anywhere in the acoustic propagation domain, which means they cannot account for the wave interactions with bodies embedded in the domain. The propagation of launch vehicle plume acoustic waves during early lift-off is heavily affected by the presence of the launch platform, flame trench and launch towers that block, reflect and diffract acoustic waves. BEM and LEE approaches do not suffer from these limitations, but they do involve linear approximations that may be ineffective at resolving nonlinearities in the acoustic propagation signature due to high speed Mach waves, and other nonlinear features predominant in the launch environment. In the end, the requirement to resolve the non-linear high amplitude, complex acoustic wave patterns from multiple plume and impingement sources and their interference with complex structures lead our team to the selection of a high-order accurate Euler solver as the appropriate tool for the CAA component.

In this paper, a two-field CFD/CAA predictive capability is presented that makes use of a well-established unstructured mesh hybrid RANS/LES solver, Loci/CHEM, and an emerging high-order accurate unstructured mesh Discontinuous Galerkin (DG) nonlinear Euler solver, Loci/THRUST, for accurately predicting and propagating acoustic waves across large distances.

The DG solver is developed in the same massively-parallel, production oriented computational framework (Loci) as the CFD solver, and solves the nonlinear Euler equations with up to 4th order spatial and temporal accuracy for improved fidelity in modeling inherently nonlinear launch-induced acoustic physics. This methodology permits acoustic predictions in the presence of obstructions in both the CFD and CAA domains and thus offers improved acoustics modeling near complex geometry, where attenuation, reflection, and diffraction are important. The CFD and CAA solvers operate on separate, but overlapping meshes and an efficient overset coupling approach is used to transmit the plume-generated acoustics from the CFD solver to the CAA solver in simultaneous execution of the two simulations.

TECHNICAL APPROACH

The development of the combined CFD/CAA simulation framework for launch vehicle liftoff acoustic environments simulation was performed under a NASA STTR Phase II project performed by a team of CFDRC researchers in cooperation with the original developers of the Loci computational simulation framework and the Loci/CHEM and Loci/THRUST simulation programs at the Mississippi State University. Details of the progression in the development, underlying computational algorithms and architectures, coupling and interfacing between the codes, and the simultaneous execution of the framework in a massively parallel fashion on NASA supercomputers has been documented in detail by the developers [10] [11] [12] [13] [14]. The components, overall CFD/CAA architecture, and coupled simulation process are summarized briefly in the following as an overview of the process.

LOCI COMPUTATIONAL FRAMEWORK

The Loci framework [15] [16] was developed with the goal of simplifying the development of complex numerical models that can take advantage of massively parallel high-end computing systems. The framework provides a rule-based programming model whereby an application is described in terms of a collection of simple computational kernels. The Loci framework can assemble these kernels and optimize their scheduling on parallel high-performance architectures. In addition, the framework is able to detect common programming errors by verifying that the algorithm conforms to a simple logical model. As a result, the Loci framework makes an excellent platform for the development and integration of a wide range of computational models. The framework supports the development of run-time loadable modules that allow Loci applications to be extended to support new physics and models with ease.

LIFTOFF PLUME IMPINGEMENT CFD: LOCI/CHEM

The Loci/CHEM code [16] [17] was developed as the first technology demonstrator for the Loci framework and has become a mature software for complex multi-physics simulations. The CHEM solver is a density-based Navier-Stokes solver employing high-resolution approximate Riemann solvers implemented for multi-component mixing and chemically reacting flows, and implicit time integration. These approaches make the CHEM solver very well-suited for compressible flow simulation. In addition, the core algorithms have been extended to accurately model flows at low speeds through the use of preconditioning techniques. The code has a variety of turbulence models including RANS and hybrid RANS/LES turbulence model treatments that include high-speed compressibility corrections. Loci/CHEM numerical models have been demonstrated to be at least second-order accurate in space and time through rigorous verification using the method of manufactured solutions (MMS). Loci/CHEM supports adaptive mesh refinement, simulations of complex equations-of-state including cryogenic fluids, conjugate heat transfer through solids, fluid-structure interaction modeling, and overset moving boundary simulations with contact detection and collision modeling to support multiple-body proximate flight in high-speed air-delivered systems.

Simulations of launch vehicle ignition and liftoff events, which use several thousand computer cores, are currently being executed using Loci/CHEM by analysts at the MSFC Fluid Dynamics Branch in support of liftoff environments definition and analysis. In production mode, simulations using Loci/CHEM are common with computational meshes exceeding 500 million cells on more than 6,000 computer cores.

FARFIELD ACOUSTIC PROPAGATION CAA: LOCI/THRUST

Loci/THRUST [18] is a density-based solver for the nonlinear Euler equations employing a Discontinuous Galerkin (DG) method capable of up to 4th order spatial and temporal solution accuracy. The DG method utilized in the Loci/THRUST solver combines some of the best features of both finite-element (FE) and finite-volume (FV) methods. Like most FE methods, the solution Q is represented by a polynomial approximation, Q_h. However, like most FV methods, the solution is assumed to be discontinuous at the interface between elements, and a Riemann problem is solved to resolve the inter-element flux contributions. Loci/THRUST offers options for Roe's approximate Riemann solver, van Leer's flux vector splitting, and local Lax-Friedrichs flux difference splitting. The temporal integration is carried out using the explicit 2^{nd}, 3^{rd} and 4^{th} order accurate strong stability preserving (SSP) TVD Runge-Kutta schemes. Loci/THRUST currently supports tetrahedral, pyramidal, prismatic, and hexahedral mesh element types.

Special attention is given to proper representation of surface discretization for the imposition of boundary conditions. The use of linear boundary surface elements to approximate a curved boundary significantly degrades the accuracy of the higher order DG solution and, in many cases, will introduce non-physical wave features into the solution. In the current Loci/THRUST DG solver implementation, the shapes of the mesh elements are represented internally as nonlinear Bézier volumes. Loci/THRUST may accept a Bezier representation of the computational mesh from mesh generation tools that offer such an option. Tools have also been developed to alternatively map existing linear grids onto a curved Bézier representation that closely aligns the grid with the actual CAD geometry or an approximation thereof.

Sponge layers are imposed in the proximity of the farfield boundaries in the DG domain. These sponge layers are designed to damp out the waves of all wavenumbers leaving the domain or reflecting back from the farfield boundaries [14].

OVERSET CFD/CAA COUPLING METHODOLOGY

The CFD/CAA coupling is applied in a one-way procedure where information is transmitted from the CFD domain to the CAA domain, and not vice-versa. The CFD and CAA domains interface with one another through overlapping mesh systems using overset domain connectivity and interpolation. The overset grid connectivity and interpolation procedure has been implemented in a completely general way to support overset grid systems of arbitrary relative spatial resolution, such that the CAA mesh may be substantially coarser than the CFD mesh if desired.

The overset coupling approach is implemented to permit runtime identification of acoustic source regions and overset grid assembly. An overset mesh *iblank* facility has been added to the Loci/THRUST code which allows non-contributing cells to be omitted from the solution process and fringe cells to be introduced at the intersection of the CFD and CAA domains. The solutions in fringe cells are interpolated from the Loci/CHEM solution to the Gauss quadrature points within the fringe cells. These values are then used to generate a set of DG solution coefficients that approximate the Loci/CHEM solution with a polynomial of the prescribed order-of-accuracy of the DG scheme. The current interface representation remains fixed during the simulation, whereas future versions of the capability will allow for dynamic overset grid assembly and identification of acoustic source regions during runtime. This will enable automatic adjustment of the overset grid assembly to an evolving plume envelope to achieve optimal proximity to the acoustic sources, while also accounting for the possibility of vehicle motion.

Given the disparities between the CFD and CAA solution procedures, the realization of an overset coupling requires both temporal and spatial interpolation from the CFD solution: spatial interpolation to obtain the CFD solution at the Gauss quadrature point locations for Fringe cells, and temporal interpolation to ensure that the spatially interpolated solution is temporally in sync with each step in the explicit Runge-Kutta procedure. A temporal sub-stepping approach is implemented that allows the implicit CFD solution to be advanced at the desired time step while the explicit CAA solution is advanced at multiple sub-steps determined by the explicit algorithm time step CFL limits. The CFL limits differ for 2nd, 3rd, and 4th order DG solutions. For the 3rd order DG simulation performed here, the CFD solution was advanced with a time step of dt=2e-6 sec, while the DG solution automatically selected on average seven sub-steps based on a CFL limit of 0.2 for the 3rd order algorithm. The selection of sub-steps is renewed at each time step and thus automatically adjusts to stability requirements as the flow field evolves.

APPLICATION AND VALIDATION CASE

As part of the CFD/CAA simulation framework development process, application testing of simulations at a production scale was initiated by software end users at the MSFC Fluid Dynamics Branch. The simulation served dual purposes: application testing and validation. The first purpose included software implementation bug fixing, maturation, full scale application testing, and full detail production level application of the newly implemented CFD/CAA framework to ensure scalability in a supercomputer production environment. This application testing resulted in numerus improvements in the implementation of boundary conditions, communications across the CFD-to-CAA interface, and simultaneous and coordinated execution of both programs. It also put the system to the test with respect to its scalability, efficiency and economy for a production application. Close cooperation between the developers and the end user test team efficiently resolved all issues identified in this process. The second purpose was the validation of the accuracy of the acoustic propagation with the CAA component and assessment of the validity of the expected increased fidelity and accuracy of the acoustic signal propagation with the CAA component.

The highly instrumented and documented ASMAT (Ares I Scale Model Acoustics Test) series of acoustics tests had previously been employed in validation of Loci/CHEM CFD liftoff environments simulations and was selected as test and validation case for the current development.

VALIDATION EXPERIMENT: ASMAT

The Ares I Scale Model Acoustics Test (ASMAT) was a series of live-fire tests of a scaled rocket motor designed to simulate the conditions of the Ares I launch configuration [20]. The ASMAT was a developmental test program led by the Propulsion Systems Department Fluid Dynamics Branch at MSFC. The primary focus of the ASMAT program was the formulation and validation of the liftoff acoustic environments definitions for the vehicle and the predicted acoustic loads. As secondary goals, it also enabled validation of analytical and computational models. In particular, the ASMAT tests provided a well-documented set of high fidelity measurements that were useful for validation of Computational Fluid Dynamics (CFD) prediction abilities. These measurements were taken over a range of test conditions and were used to validate CFD prediction of phenomena like Ignition Over-Pressure (IOP) and the effectiveness of deluge water sound suppression on the liftoff environment.

The fully assembled ASMAT test article included five-percent scale models of the Ares I launch vehicle and propulsion systems. The ground systems and water sound suppression systems were also modeled at five-percent scale. Two Alliant Techsystems Inc. (ATK) Rocket Assisted Take-Off (RATO) motors were selected to represent the Five-Segment Reusable Solid Rocket Motors (RSRMV). The RATO motors required a nozzle extension in order to reach the correct scale nozzle exit diameter. The test included water sound suppression systems above

and below the mobile launcher platform and inside the exhaust hole. Simulations presented in this paper were performed for tests without any water injection.

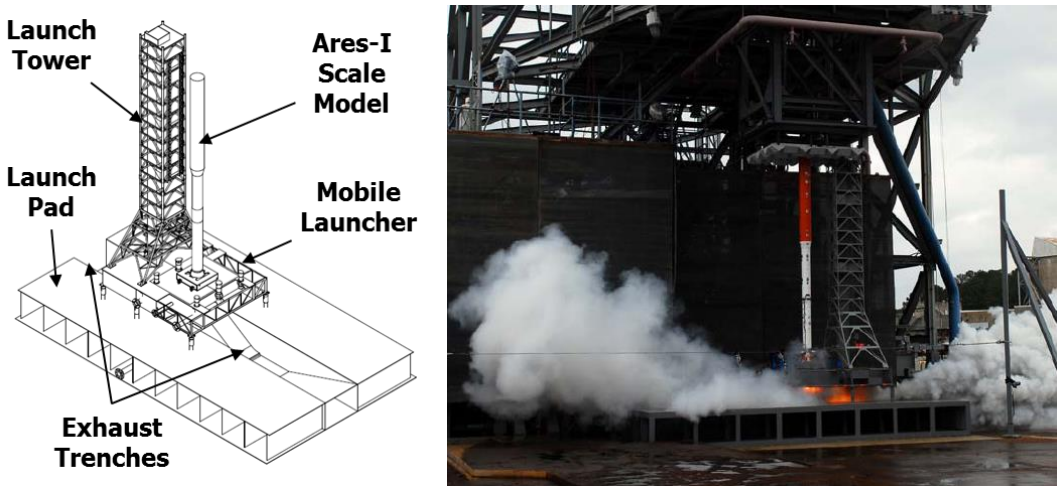

Figure 1: ASMAT - Ares I Scale Model Acoustic Test

COMPUTATIONAL MODEL

The computational model assembled to validate the hybrid CFD/CAA approach required the generation of two models, one for the CFD domain solution and one for the CAA solver domain with appropriately placed interfaces. For the CFD simulation part, a previously generated ASMAT CFD model was employed with the best practices in place for liftoff acoustic environment with the Loci/CHEM CFD framework. This model represents the practical production case level of mesh resolution of our current liftoff CFD simulations.

CFD PLUME FLOW DOMAIN MODEL

The CFD model for the ASMAT simulation was created from the CAD model of the actual test stand configuration. Figure 2 shows an overall view of the level of detail contained in the CFD model. The internal volume of the RATO motor nozzle is modeled reaching upstream into the combustion chamber section where the inflow boundary conditions are imposed. This allows the flow through the nozzles to be directly computed, in particular to correctly capture the evolution of the RATO nozzle start-up flow transients.

The computational volume mesh for the simulation was generated as a hybrid mesh, featuring an unstructured tetrahedral volume mesh with a clustered prismatic viscous boundary layer mesh advancing from an unstructured wall surface mesh. The AFLR3 (3-D Advancing Front and Local Reconnection) mesh generator was applied [22]. The volume mesh contained a total of 378M mesh cells predominantly resulting from the high mesh resolution imposed in the plume region under the launch pad to resolve the acoustic source regions and mesh resolution along the length of the vehicle. Mesh cell size in the plume region was approximately 0.1 inch. Mesh cell sizes of approximately 0.3 inch were used around the vehicle. The mesh in this region around the vehicle was meshed more evenly and with slightly better resolution than in previous ASMAT validation projects [19] [21] to ensure proper spatial resolution along the entire signal travel distance. The remainder of the mesh coarsens progressively towards the farfield domain boundaries for efficiency. The overall domain mesh is shown in Figure 3, the resolution of the regions near the vehicle and tower are shown in Figure 4, and the highly resolved plume region mesh is shown in Figure 5.

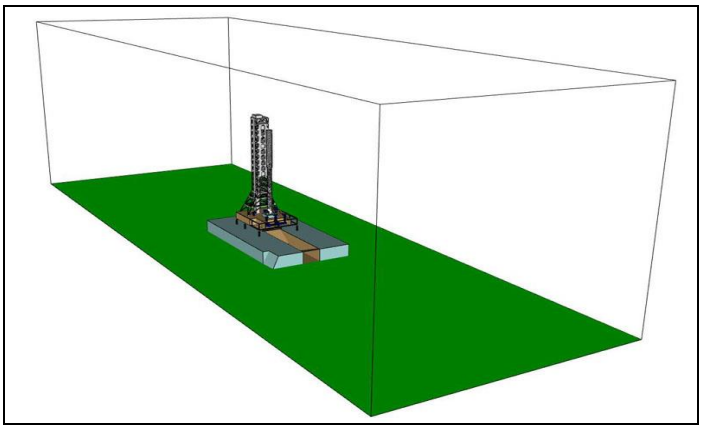

Figure 2: ASMAT CFD Model Domain

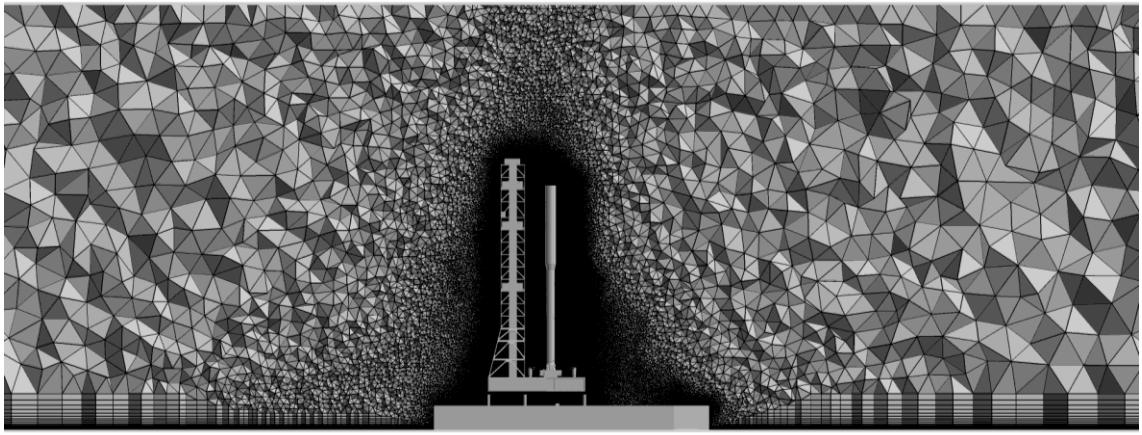

Figure 3: Center plane cut through CFD mesh.

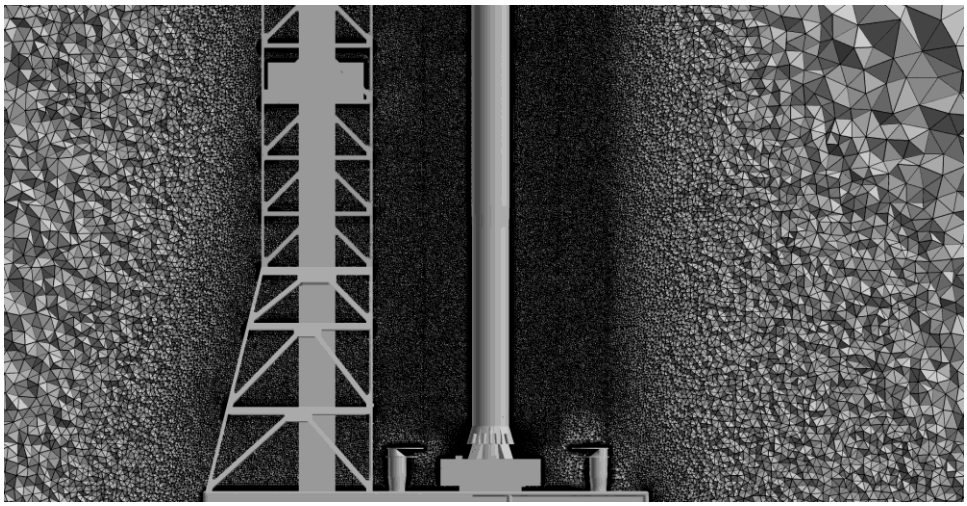

Figure 4: Center plane cut through CFD mesh near vehicle on launch mount.

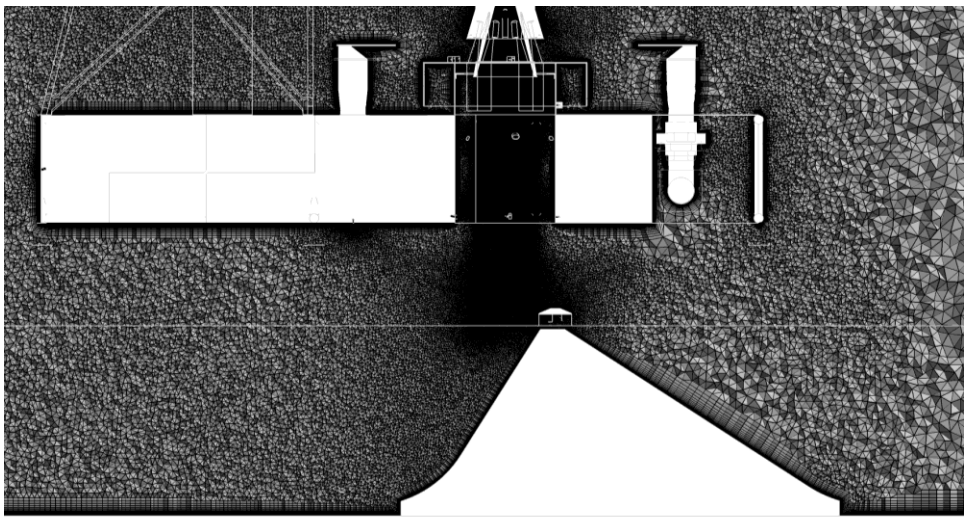

Figure 5: Center plane cut through CFD mesh in plume impingement region under ML.

ASMAT MOTOR NOZZLE TRANSIENT INFLOW BOUNDARY CONDITION

The CFD simulation was performed with a non-reacting chemistry model that consists of air at atmospheric conditions and a 'heavy gas' equivalent species approximation of the RATO combustion gas and particulate phase constituent mixture thermodynamics. The use of a single equivalent plume gas species for each component has proven to be sufficiently accurate and economical in previous applications.

The RATO motor inflow was modeled with a prescribed time dependent mass flow profile boundary condition on a plane slightly upstream of the converging portion of the RATO nozzle. Since the actual mass flow profile of the RATO motors was not known, a transient boundary condition for the RATO nozzle flow was developed utilizing an approximate chamber pressure time profile obtained from strain gauges on the RATO casing, assuming a proportional relationship between mass flow rate and measured chamber pressure. This approach is outlined in detail in Casiano [19]. The motor start-up profile shows the familiar solid motor characteristics with an initial igniter induced mass flow ramp-up and leveling to a low level flow, followed by the rapid rise in mass flow and pressure as the full motor ignition sets in.

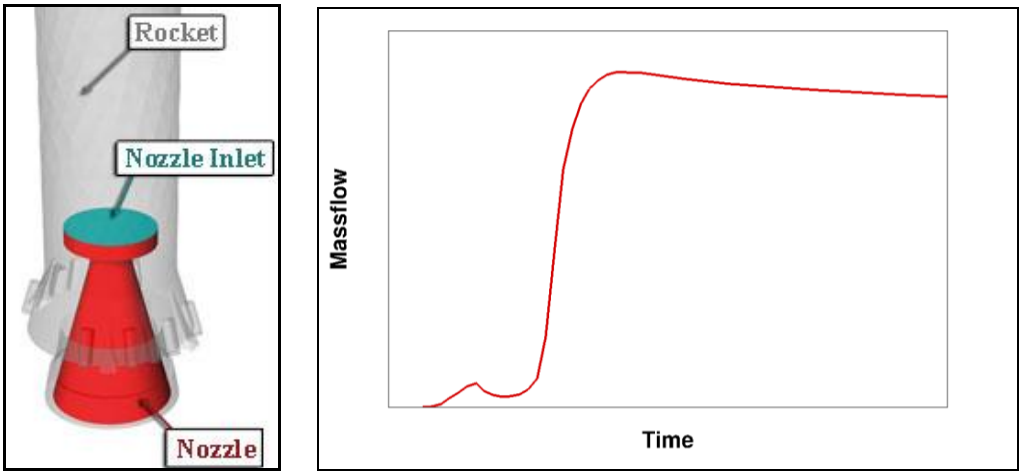

Figure 6: ASMAT Nozzle Inlet Mass Flow Boundary Location and Start-up Mass Flow Profile [20]

Imposing a bulk mass flow boundary condition lacks the three-dimensionality and turbulence features of the flow exiting the combustion section and entering the nozzle at the imposed boundary. The transient turbulence features forming inside the nozzle are captured by the hybrid RANS/LES simulation of the nozzle flow, but fail to account for the dynamics arriving from the motor internals. For future applications, a more accurate approach will be used that directly extracts a time dependent flow profile generated from a separate CFD simulation of the internal RATO ignition and nozzle outflow flow field formation. Such RATO internal transient ballistic simulations are ongoing work and results are still being vetted. This approach has been applied in subsequent Space Launch System (SLS) simulations [22] and confirmed the increased fidelity of such an approach.

The simulation was performed with the proven and validated Loci/CHEM algorithm, which is second order accurate in space and time. This approach provides the robustness required for capturing the complex multi-species turbulent plume impingement flow fields and offers sufficient accuracy to capture the unsteady turbulence and acoustic wave source regions around the plumes on properly resolved meshes. The propagation of the acoustic field with this algorithm to the farfield regions towards the upper regions of the launch vehicle results in appreciable numerical dissipation of the signal content, as will be shown. This effect is exacerbated by the need to limit total computational mesh size by coarsening the mesh in the farfield away from the plume regions.

CAA SIMULATION DOMAIN MODEL

As this exercise constituted a first application test of the new simulation framework, the CAA model was somewhat simplified to save computational cost and quicken turn-around for this first application test. For example, the rainbird deluge water nozzles on the mobile launcher deck were omitted and the mobile launcher platform was approximated as a rectangular box by omitting various cut-outs on the platform sides. The main features such as the vehicle, the launch mount opening and the tower were retained with nearly all details.

The CAA mesh was generated as an inviscid flow mesh without any boundary layer clustering. The CAA mesh also featured a larger mesh cell size of approximately 0.75 inch on average, compared to a CFD mesh size closer to 0.3 inch in the regions around the vehicle and tower. When overlaid on each other, the outer mold line of the mobile launcher, vehicle and tower provide essentially the same feature resolution as shown in Figure 7. The CAA domain, depicted in light blue, only extends across the footprint of the launch pad to receive acoustic signal influx from the top opening of the flame trench. The CFD domain extends to a much larger distance to resolve and accommodate the plume flow. The CFD farfield domain boundaries are placed at a distance sufficient to not impede expansion of the plume flow out of the flame trench to the farfield and avoid boundary condition induced wave reflections.

Figure 8 indicates how the CAA domain wraps around the mobile launcher body and extends to a four-sided interface boundary close to the exhaust opening at the bottom of the mobile launcher platform and the edge of the flame trench opening. The four sided interface and the CAA domain surface over the flame trench opening describe the region where overset hole cutting is to be applied, which then introduces fringe cells for use in receiving acoustic signal inflow from the CFD domain. The CAA domain reaches into the vehicle launch mount opening to a level just above the motor nozzle exit to also serve as overset acoustic influx interface. The CAA domain extends the full height of the tower and the top and side domain boundaries are designated as non-reflecting boundaries. The non-reflecting characteristics are enforced by the acoustic signal sponge layer inside the boundaries.

An unstructured tetrahedral cell computational mesh is used in the CAA domain with cell sizes in the range from 0.5 to 1.5 inch. The cell size near the vehicle was approximately 0.75 inch. Mesh cells near the vehicle aft end in proximity with the launch mount featured locally slightly higher resolution down to approximately 0.25 inch. The mesh was designed for an inviscid

Euler solution with no boundary mesh clustering. The mesh contained a total of 40M tetrahedral cells. Figure 9 shows a cut of the mesh through the vehicle and flame trench symmetry plane.

The cell size for the DG solver mesh was chosen larger than in the CFD mesh. The DG solution utilizes internal degrees of freedom in resolving each computational cell. The DG solver increases the cell resolution to 8 degrees of freedom for hexahedral cells and 4 for tetrahedral cells with the 2nd DG solution. Resolution increases to 27 degrees of freedom for hexahedral cell and 10 for tetrahedral cells with the 3rd order DG solution applied in this work. It increases to 64 and 20 degrees of freedom, respectively for a 4th order solution [18]. The spatial resolution for a wave traversing across a 3rd order DG tetrahedral mesh cell would therefore be on the order of one third the cell size (i.e., ten degrees of freedom resulting in approximately three degrees in each dimension). This allowed the selection of the DG solution mesh with a cell size near 0.75 inch to offer spatial resolution on par with to a CFD mesh resolution in the 0.3 inch range.

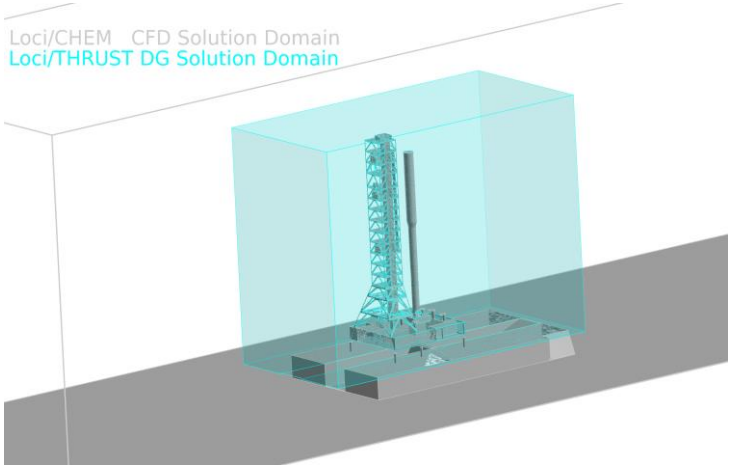

Figure 7: Overlay of DG domain embedded in CFD domain. Note cut outs on DG domain boundaries resulting from overset interfaces.

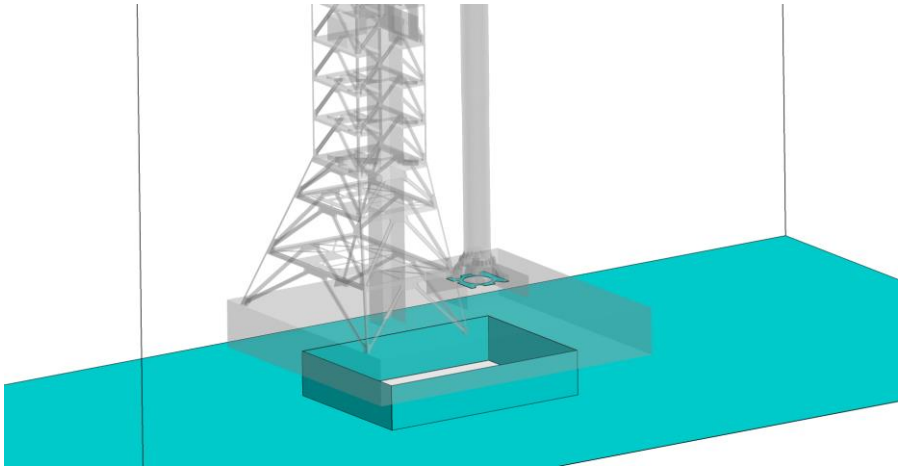

Figure 8: DG domain Interface boundaries receiving input from CFD solution through overset mesh connectivity: 1) plane above nozzle inside ML exhaust duct; 2) four sided enclosure of plume region under ML; 3) surface spanning pad surface and top opening of flame trench.

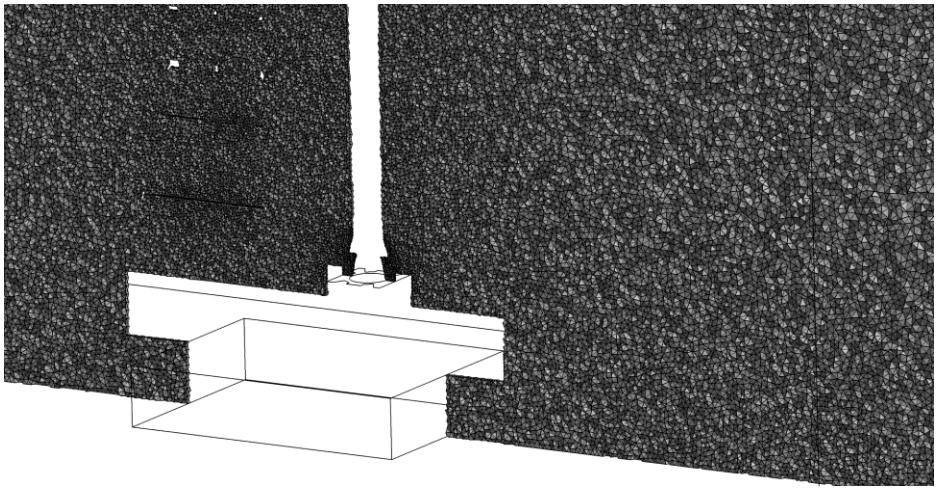

Figure 9: Computational volume mesh planar cut showing mesh resolution for DG solution.

COUPLED CFD/CAA SIMULATION EXECUTION

The simulation was executed on the NASA Pleiades supercomputer at the NASA Ames Research Center NAS facility. The simulation presented here was executed on 1600 computer cores. Both the Loci/CHEM CFD solution and the Loci/THRUST 3rd order CAA solution were executed on the same set of cores. No processors were thus ever idle during the simulation. The sequential execution of the two programs and the necessary information exchange was coordinated by the Loci CFD/CAA framework.

The physical time step for the simulation was specified to be dt = 2e-6 sec to be comparable with the high definition microphone sample rates in the validation data sets. The simulation was executed with 3rd order accurate settings for Loci/THRUST. The stability limit recommendation of CFL=0.2 for the 3rd order solution on the current mesh led the framework to select seven Loci/THRUST sub-steps on average for each Loci/CHEM step. Each total simulation time step required approximately 75 sec of CPU time for each physical time step. The simulation covering a real time of 25 milliseconds thus required approximately 11 days of total computational time using 1600 processors. The computational cost is broken down into 40 % for the CHEM solution and 60% for the DG solution. The overall computational expense and simulation turn-around time remains reasonable considering the crucial gains from the acoustic prediction accuracy.

RESULTS AND DISCUSSION

The simulation was executed for a total of approximately 25 milliseconds from the time the motor internal flow arrives at the inflow boundary in the CFD model. This time was sufficient to sample acoustic data for the sensors located along the length of the vehicle and assess the differences between the CFD, CAA and experimental acoustic signal characteristics. The motor has not reached full power yet at the end of simulation. The simulation thus only compares acoustic events during the ignition overpressure field formation phase and does not capture the maximum launch acoustic levels. Processing of the simulation and the experimental signal data was performed only for the simulated time span. The experimental data thus does not contain the occurrence of the maximum acoustic loads levels and frequency at a later time.

SIMULATION RESULTS

Figure 10 shows a time sequence of side-by-side simulation snap shots from an animation of the CFD and CAA simulation pressure field in the center plane along the flame

trench. The comparison shows that the overset connectivity between the simulations properly passes the transient flow development with both spatial and temporal accuracy.

This is confirmed in a more detailed side by side comparison of the pressure field contours at the end of the simulation shown in Figure 11. The near identical contours in the vicinity of the mobile launcher platform indicate that the CFD simulation information is faithfully transmitted to the CAA simulation. Significant losses in resolution of the pressure contours occur for the CFD in the coarsened mesh regions away from the vehicle and tower region. The DG solver mesh is both coarser and evenly distributed and can resolve the details more efficiently and conservatively.

The DG solution domain in Figure 11 also shows the effectiveness of the sponge layers activated near the farfield domain boundaries. The signals are effectively dampened out and no reflection back into the solution domain occurs.

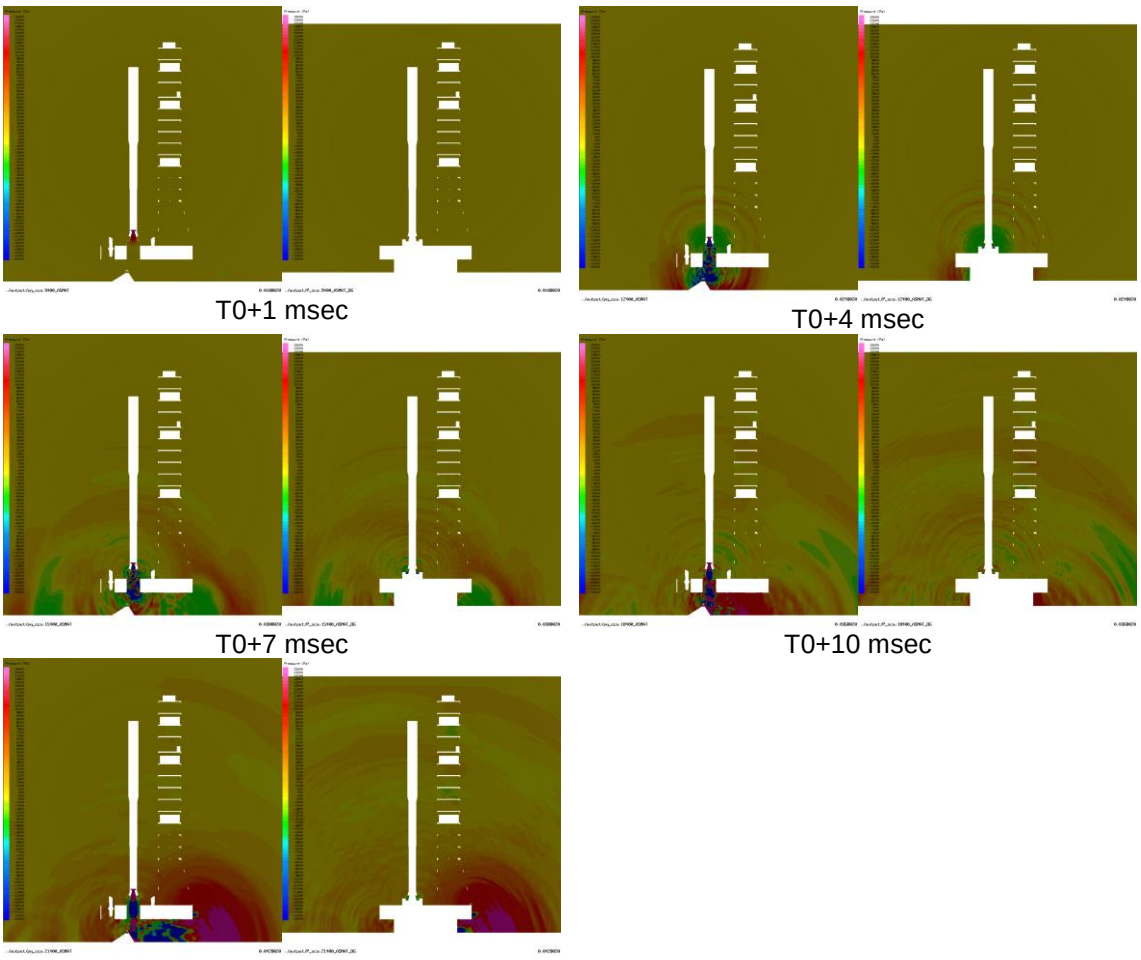

Figure 10: Comparison of Pressure Wave Development during Ignition Sequence. Left: Loci/CHEM Solution; Right: Loci/THRUST 3rd Order Solution

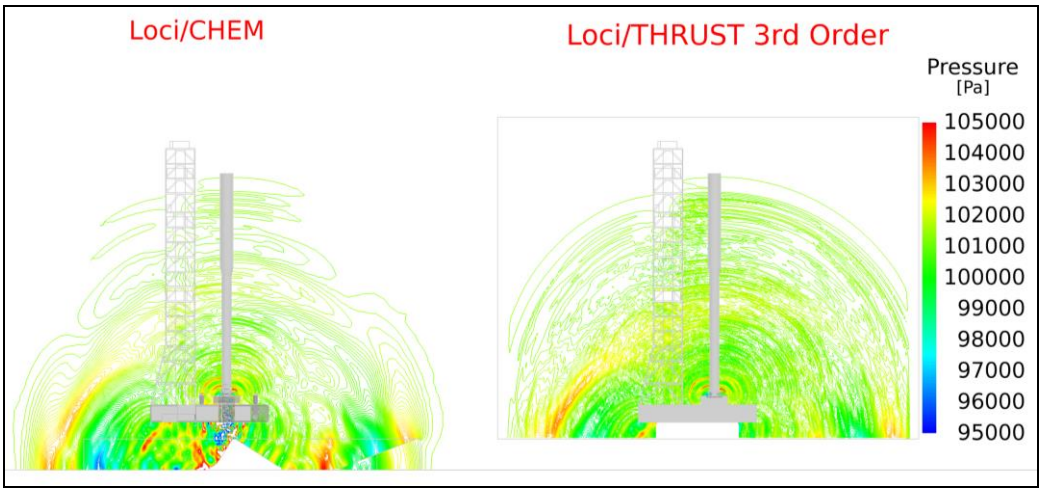

Figure 11: Comparison of Pressure Wave Field Resolution near End of Simulation. Left: Loci/CHEM Solution; Right: Loci/THRUST 3rd Order Solution

COMPUTED ACOUSTIC SIGNAL FREQUENCY SPECTRUM

The ASMAT test was equipped with numerous pressure sensors on the vehicle and the launch pad components. The CFD model was equipped with data probe points at the respective sensor locations. Data was sampled at those probe locations at every time step during the CFD simulation, resulting in a sample rate of 500,000 Hz. The sensors on the test featured two sample rates, at 4,000 Hz and 256,000 Hz. A comparison of the signals computed and measured is presented in the following for two sensor locations equipped with high sample rate sensors. The first sensor is located on the vehicle aft skirt in close proximity of the mobile launcher launch mount opening. The second sensor location is at the very top of the vehicle. The first location features a fairly well resolved CFD mesh and a short signal travel distance from the plume. This location is thus an example of the best results that can be expected from a pure CFD simulation to capture the acoustic content. The second location features a long signal travel distance which has been shown in previous CFD validations to result in considerable loss of frequency content due to numerical dissipation. The signal reaching this sensor has furthermore traveled through mesh regions that have been slightly coarsened to keep the simulation computationally affordable for production application schedules.

Figures 12 and 13 indicate that the simulations generally capture all major low frequency wave events occurring during this nozzle start-up and plume formation phase recorded in the test data such as igniter pulse, ignition over-pressure and duct over-pressure waves. However, there are discrepancies in the timing and amplitudes of some events. The experimental data displays significantly higher amplitude content early in the start-up sequence compared to the simulations. The simulations result in high amplitude events later in the simulations at a time when the experimental data has settled down to lower amplitude levels. We attribute these discrepancies to the lack of fidelity of the motor mass flow boundary condition. Recall that the simulation inflow boundary condition was imposed as bulk mass flow boundary condition that does not contain the highly energetic flow features resulting from the internal motor start-up ballistics arriving at this location. The flow originating from the mass flow boundary condition is energized during the CFD simulation through the hybrid RANS/LES turbulence modeling of the highly transient nozzle filling sequence. This resulted in generation of the high amplitude and higher pressure level signals occurring later in the CFD data. As mentioned, a more physically accurate approach to the boundary condition will be used for future applications that directly extracts a time dependent flow profile generated from a separate CFD simulation of the internal RATO ignition and nozzle outflow flow field formation.

There is a noticeable deviation in the signal shape between the CFD and CAA simulation at the upper vehicle sensor location. Recall that the CAA model featured a simplified mobile launcher platform shape in the form of a box shape enclosing the mobile launcher platform maximum dimensions. The actual test configuration and the CFD model feature various open volume areas on the sides and over the flame trench. The increased blockage results in a longer path and the CAA signal arrival being delayed at the sensor location. This simplified CAA geometry model was accepted in light of the initial application testing scope of this simulation.

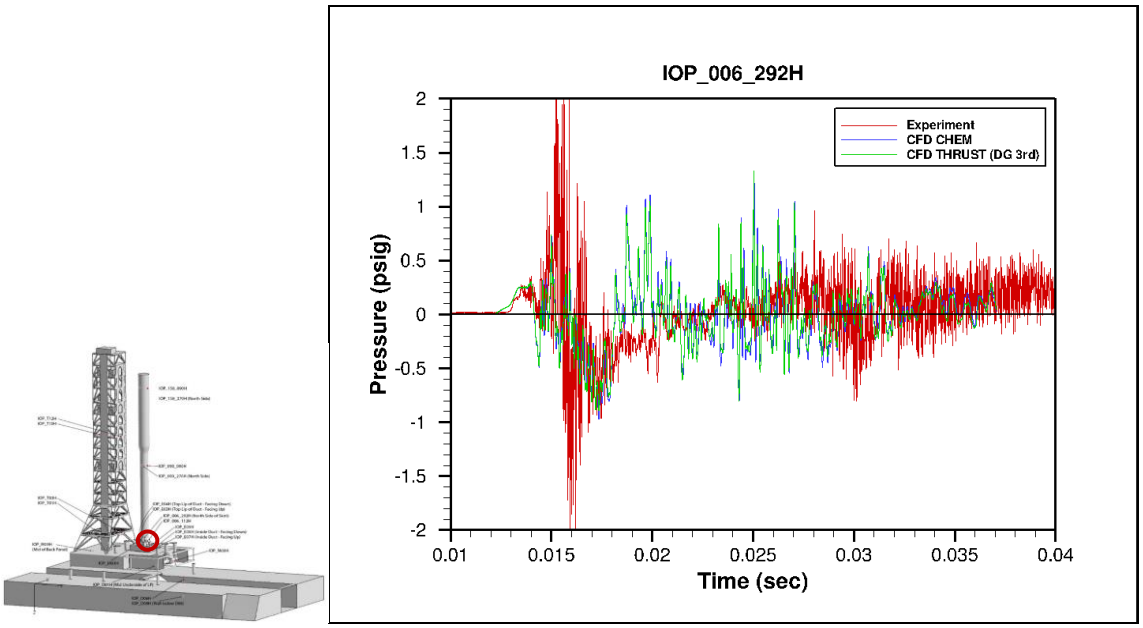

Figure 12: Pressure Signal Profile at Vehicle Base for First 25 msec after Ignition

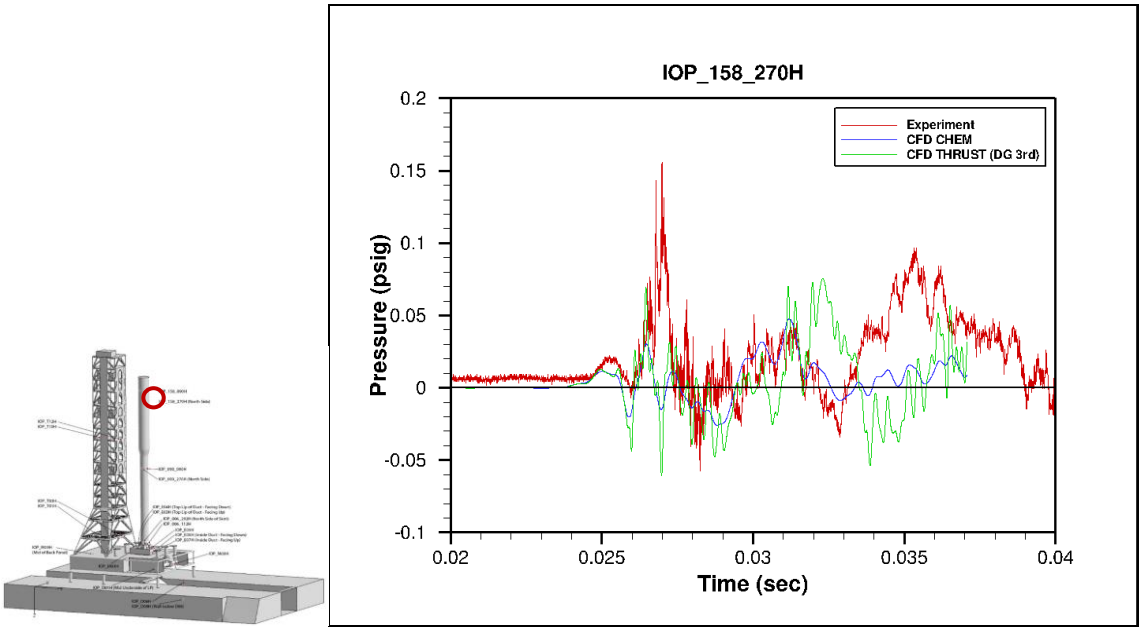

Figure 13: Pressure Signal Profile near Vehicle Top for First 25 msec after Ignition

Next, comparisons are presented at the two pressure sensor locations against high sample rate test data. The pressure data from the CFD simulation and the test data were transformed to the frequency domain using the Fourier transform and a Hamming filter function was used to taper the data. The Nyquist frequency (half the sampling rate) was 128 kHz for the high sample rate test data and 250 kHz for the CFD data. The frequency spectrum is presented in the following figures in the form of Sound Pressure Level (SPL) as a function of frequency.

Well-established rules in CFD-based acoustic environments analysis dictate a resolution of 15 to 20 mesh cells for each wavelength to properly resolve acoustic waves with a second order accurate CFD solver. The Loci/CHEM simulation should therefore be able to resolve frequencies in the range of 6,000 to 9,000 Hz in the mesh region near the plumes (0.1 inch cell size), and in the range of 2,200 to 3,000 Hz in the regions around the vehicle (0.3 inch cell size).

The frequency spectra at the sensor location at the aft end of the vehicle are shown in Figure 14. These sensors are located in regions with a reasonably well and evenly resolved CFD mesh. The CFD and CAA sensors show capacity to resolve frequency content up to 8,000 Hz matching the experimental data. The mesh resolution for the CFD or the CAA simulations is however not sufficient to resolve frequencies beyond this level. The CAA solution remains closer to the experimental data, whereas the CFD data dramatically drops off. The ability of both the CFD solver and the DG solver to reliably resolve high frequency content between 1,000 Hz to 8,000 Hz on an adequately sized mesh is an important validation result. This confirms the previously verified accuracy of the Loci/CHEM solver of second order or better. The simulation results agree extremely well with the experimental data across all frequencies below the mesh resolution threshold. This gives confidence in the correct physics modeling setup of our liftoff simulation models.

Figure 15 show the frequency spectra at the sensor location at the top of the vehicle model. Again the CAA solution is able to track the signal up to a frequency above 7,000 Hz and close to 8,000 Hz before again dissipating the signal due to lack of mesh resolution. The CFD signal, however, fails to resolve frequencies beyond 1,000 Hz. The dissipative character of the CFD solver numerics in propagation of the signal over the vehicle length distance becomes very apparent at this sensor location. The absence of high frequency signal content is apparent in the CFD pressure signal trace in Figure 13. The DG solver has no problem in properly resolving and preserving the acoustic wave content. Good agreement in validation against the experimental data is again observed for the CFD and DG solutions in their respective properly resolved frequency ranges.

The application test validation thus confirmed the superior performance delivered by the higher order CAA solver for acoustic field simulations. The gains demonstrated by the 3rd order DG solution are expected to further increase by extension to the 4th order solver. The higher order solver will be tested as soon as the higher order wall boundary conditions under development are fully operational. Optimal performance towards maintaining higher frequency signals will be driven by a combination of higher order resolution and mesh cell size reduction to accommodate the higher frequency wave lengths.

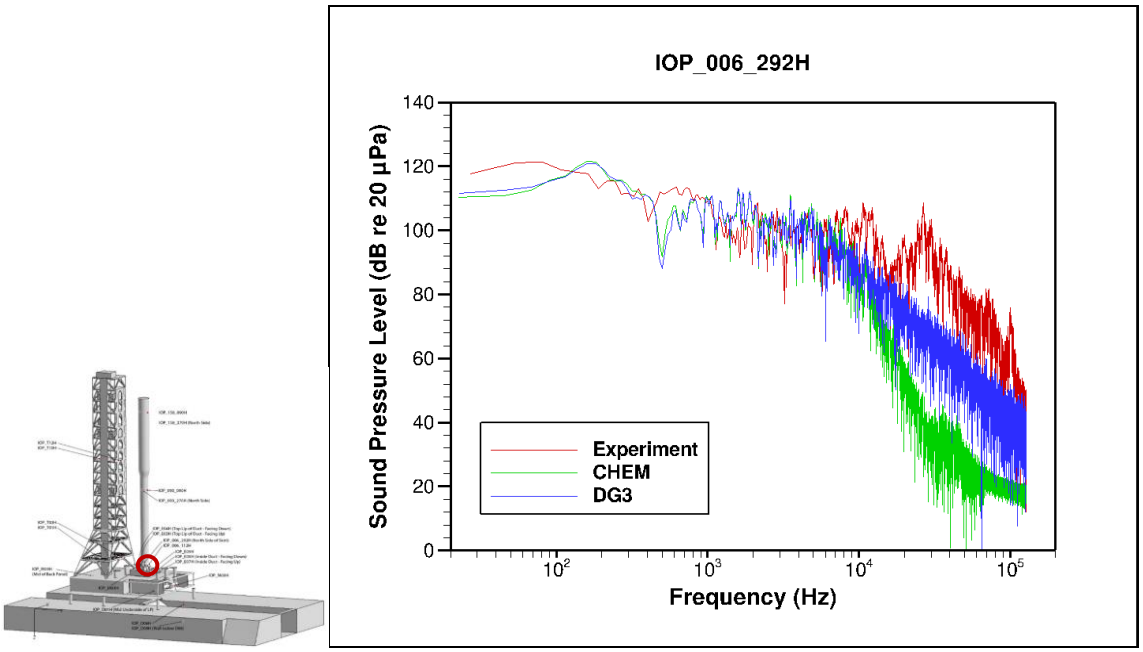

Figure 14: Sound Pressure Level Acoustic Profile at Vehicle Base for first 25 msec after Ignition

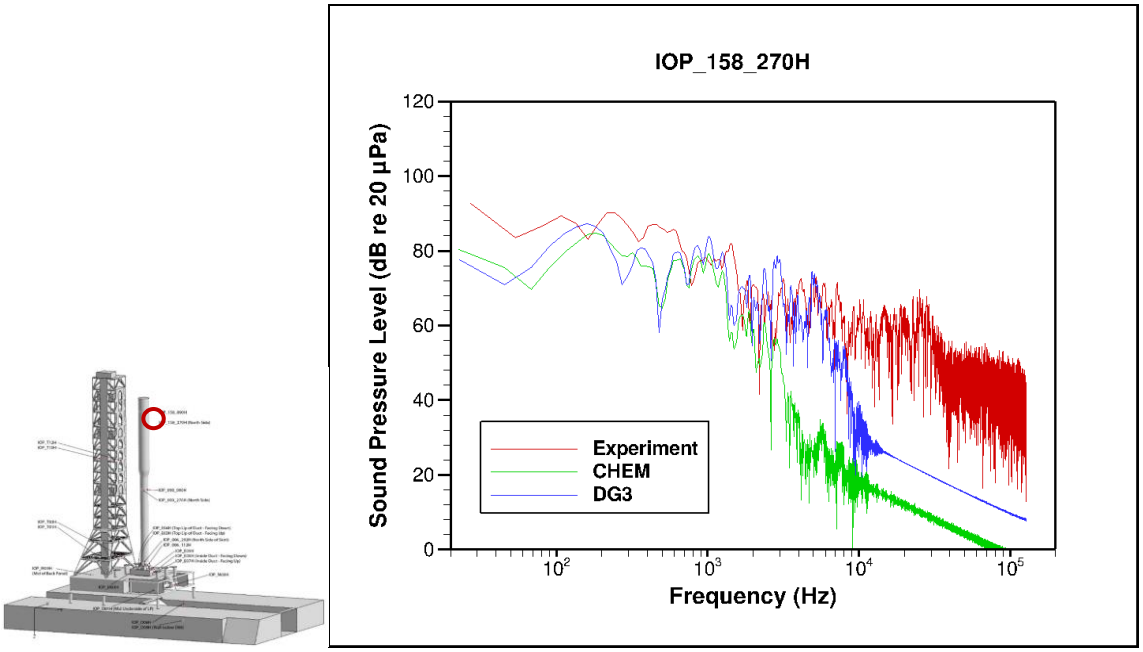

Figure 15: Sound Pressure Level Acoustic Profile near Vehicle Top for first 25 msec after Ignition

SUMMARY AND CONCLUSIONS

We have developed a hybrid CFD and computational aero-acoustics (CFD/CAA) modeling framework to improve liftoff acoustic environment predictions. The framework combines the existing, highly scalable NASA CFD code, Loci/CHEM, with a high-order accurate Discontinuous Galerkin (DG) solver, Loci/THRUST, developed in the same framework. Loci/THRUST employs a low-dissipation, high-order, unstructured DG method to accurately propagate acoustic waves away from the source regions across large distances. The DG solver can provide up to fourth-order accurate solutions for non-linear, conservative acoustic field propagation. Higher-order boundary conditions are implemented to accurately model the reflection and refraction of acoustic waves on launch pad components. The DG solver accepts generalized unstructured meshes, enabling efficient application of common mesh-generation tools for CHEM and THRUST simulations. The DG solution is coupled with the CFD solution by means of overset grid assembly and interpolation from the CFD acoustic source regions.

Initial software testing and validation of the higher-order acoustic propagation simulation technique was accomplished via comparison with acoustic data from the Ares I Scale Model Acoustic Test (ASMAT) experiments performed at NASA's Marshall Space Flight Center. This validation simulation served to evaluate the capabilities and production readiness of the CFD/CAA framework toward resolving the experimentally observed spectrum of acoustic frequency content. Many improvements to the numerical algorithm, boundary conditions, and communication process between the simulations were identified and implemented. Our initial simulations were performed with the third-order DG solver. Testing with the fourth-order solver will commence as soon as higher-order boundary conditions have been fully implemented.

Application of this two-field CFD/CAA simulation approach proved to be practical and reasonably economical for the test simulation performed in this work. The practicality of coupling and simultaneously executing the CFD and CAA modules within a single simulation is a major benefit enabled by the Loci computational framework. The simultaneous execution of the DG solver for the CAA simulation more than doubled the CPU time compared to a stand-alone CFD simulation. The overall computational expense and simulation turn-around time remains reasonable considering the crucial gains from the acoustic prediction accuracy.

The low dissipation, higher order spatial and temporal accuracy of the DG solution facilitates propagation of high frequency noise signals over extreme distances of the size of a launch pad. This enables the capture of the important liftoff peak vehicle acoustic loads that occur in the higher frequency ranges in the 5,000 to 10,000 Hz range for scale model tests such as ASMAT. Tracking high frequency signals over long distances of the size of a vehicle on a launch pad has so far been elusive for CFD simulations.

This improved capability to perform high fidelity computational acoustic field simulations increases confidence in the specification and understanding of launch acoustic loads design environments. Understanding of the acoustic environments can now be expanded beyond the data available from the limited number of sub-scale tests that could be performed for ASMAT and the current Scale Model Acoustic Test (SMAT) for the Space Launch System (SLS). Numerical simulations can be applied in evaluating various sound suppression measures, reducing the need for expensive testing.

REFERENCES

1. Lighthill, M. J., "On Sound Generated Aerodynamically - Part I. General Theory," *Proc. of the Royal Society of London* , Vol. 211, 1952, pp. 564-587.
2. Lighthill, M. J., "On Sound Generated Aerodynamically - Part II. Turbulence as a Source of Sound," *Proc. of the Royal Society of London*, Vol. 212, 1955, pp. 1-32.

3. Farassat, F., “The Kirchhoff formulas for moving surfaces in aeroacoustics - the subsonic and supersonic class,” *NASA Technical Memorandum 110285,* 1996.

4. Williams, J. E. F. and Hawkings, D. L., “Sound Generation by Turbulence and Surfaces in Arbitrary Motion,” *Phil. Trans. of the Royal Society*, Vol. A264, 1969, pp. 321–342.

5. Advanced CAE Research, L., “FastBEM Acoustics,” http:www.//fastbem.com, (2007).

6. Bailly, C. and Juve, D., “Numerical solution of acoustic propagation problems using linearized Euler equations,” *AIAA Journal*, Vol. 38, No. 1, 2000.

7. Bogey, C., Bailly, C., and Juve, D., “Computation of flow noise using source terms in linearized Eulers equations,” *AIAA Journal*, Vol. 40, No. 2, 2002.

8. Della, R., Rinaldi, R., Iob, A., and Arina, R., “An efficient Discontinuous Galerkin method for aeroacoustic propagation,” *International Journal for Numerical Methods in Fluids* , Vol. 69, No. 9, 2012, pp. 1473-1495.

9. Bauer, M., Dierke, J., and Ewert, R., “Application of a Discontinuous Galerkin Method to Discretize Acoustic Perturbation Equations,” *AIAA Journal*, Vol. 49, 2011, pp. 898–908.

10. Harris, R., Collins, E., Luke, E., Sescu, A., Strutzenberg, L., and West, J., “Hybrid Discontinuous Galerkin and Finite Volume Method for Launch Environment Acoustics Prediction," AIAA Journal, Vol. 53, No. 11 (2015).

11. Harris, R., Collins, E., Luke, E., and Sescu, A., “Coupled Overset Unstructured Discontinuous Galerkin Method for Launch Environment Acoustics Prediction," AIAA Journal, Vol. 54, No. 6 (2016).

12. Harris, R., Sescu, A., Collins, E., and Luke, E., "Coupled Overset Unstructured Discontinuous Galerkin Method for Jet Noise Prediction," 54th AIAA Aerospace Sciences Meeting, AIAA SciTech, AIAA Paper 2016-0762 (2016).

13. Harris, R., Arslanbekov, R., Collins, E., and Luke, E., "Validation of Overset Discontinuous Galerkin and Hybrid RANS/LES Method for Jet Noise Prediction," 46th AIAA Fluid Dynamics Conference, AIAA Aviation, AIAA Paper 2016-3334 (2016).

14. Sassanis, V., Sescu, A., Collins, E., Harris, R., and Luke, E., “Hybrid Approach to Nonlinear Propagation of Jet Noise in Complex Environments,” 54th AIAA Aerospace Sciences Meeting, AIAA SciTech, AIAA Paper 2016-0528 (2016).

15. Luke, E. 2005. "Loci: a rule-based framework for parallel multi-disciplinary simulation synthesis." Journal of Functional Programming 15 (3): 477-502.

16. E. Luke, X-L. Tong, J. Wu, L. Tang, and P. Cinnella, "A Step Towards `Shape Shifting' Algorithms: Reacting Flow Simulations Using Generalized Grids," 39th AIAA Aerospace Sciences Meeting and Exhibit, January 8-11, 2001, AIAA Paper 2001-0897.

17. Luke, E. 2007. "On Robust and Accurate Polytype CFD Solvers." 18th AIAA Computational Fluid Dynamics Conference. Miami: AIAA 2007-3956.

18. Collins, E., “On Mesh Quality Considerations for the Discontinuous Galerkin Method,” Ph.D. Thesis, Mississippi State University, 2009.

19. Casiano, M.J., McDaniels, D.M., Alvord, D.A., and Putnam, G.C., “Ares I Scale Model Acoustic Test Overpressure Final Analysis,” NASA/TP-2013-217478 (2013).

20. Casiano, M.J.; McDaniels, D.M.; and Alvord, D.A.: “Five Percent Ares I Scale Model Acoustic Test Overpressure Characterization and Analysis,” 162nd Meeting of the Acoustical Society of America, San Diego, CA, October 31–November 4, 2011.

21. Putnam, G.: “Validation and Simulation of Ares I Scale Model Acoustic Test - Pathfinder Development,” 8th JANNAF Modelling and Simulation Subcommittee Meeting, Huntsville, AL, December 6, 2011.

22. Davis, P., Putnam, G., and Williams, B., “Simulating Rocket Ignition and Launch Environments for NASA’s Space Launch System,” SC13 – 13th International Conference for High Performance Computing, Networking, Storage and Analysis, Denver, CO, Nov 2013.

23. Marcum, D.L. and Gaither, J.A., “Mixed Element Type Unstructured Grid Generation for Viscous Flow Applications.” 14th AIAA Computational Fluid Dynamics Conference, AIAA Paper 99-3252, (1999).